Materials Today Chemistry 17 (2020) 100272

Contents lists available at ScienceDirect

Materials Today Chemistry

journal homepage: www.journals.elsevier.com/materials-today-chemistry/

Peptide nucleic acid stabilized perovskite nanoparticles for nucleic acid sensing

A. Jancik Prochazkova [a, b], S. Gaidies [c], C. Yumusak [a], O. Brüggemann [c], M. Weiter [b], N. S. Sariciftci [a], M. C. Scharber [a], K. Čépe [d], R. Zbořil [d], J. Krajcovic [b], Y. Salinas [c, *], A. Kovalenko [a, b, **]

[a] Linz Institute for Organic Solar Cells (LIOS), Physical Chemistry, Johannes Kepler University Linz, Altenberger Straße 69, 4040, Linz, Austria
[b] Faculty of Chemistry, Materials Research Centre, Brno University of Technology, Purkyňova 118, 612 00, Brno, Czech Republic
[c] Institute of Polymer Chemistry (ICP), Johannes Kepler University Linz, Altenberger Straße 69, 4040, Linz, Austria
[d] Palacký University Olomouc, Regional Centre of Advanced Technologies and Materials, Šlechtitelů 27, Olomouc, Czech Republic

ARTICLE INFO

Article history:
Received 18 December 2019
Received in revised form
31 March 2020
Accepted 1 April 2020
Available online xxx

Keywords:
Thymine-based peptide nucleic acid
Hybrid lead bromide perovskite nanoparticles
Adenine nucleic acid sensing
Thin films

ABSTRACT

Nanostructural hybrid organic-inorganic metal halide perovskites offer a wide range of potential applications including photovoltaics, solar cells, and light emitting diodes. Up to now the surface stabilizing ligands were used solely to obtain the optimal properties of nanoparticles in terms of dimensionality and stability, however their possible additional functionality was rarely considered. In the present work, hybrid lead bromide perovskite nanoparticles (PNP) were prepared using a unique approach where a peptide nucleic acid is used as a surface ligand. Methylammonium lead bromide perovskite colloidal nanoparticles stabilized by thymine-based peptide nucleic acid monomer (PNA-M) and relevant trimer (PNA-T) were prepared exhibiting the size below 10 nm. Perovskite structure and crystallinity were verified by X-ray powder diffraction spectroscopy and high resolution transmission electron microscopy. PNP-PNA-M and PNP-PNA-T colloidal dispersions in chloroform and toluene possessed green-blue fluorescence, while Fourier-transform infrared spectroscopy (FT-IR) and quantum chemical calculations showed that the PNA coordinates to the PNP surface through the primary amine group. Additionally, the sensing ability of the PNA ligand for adenine nucleic acid was demonstrated by photoluminescence quenching via charge transfer. Furthermore, PNP thin films were effectively produced by the centrifugal casting. We envision that combining the unique, tailored structure of peptide nucleic acids and the prospective optical features of lead halide perovskite nanoparticles could expand the field of applications of such hybrids exploiting analogous ligand chemistry.

1. Introduction

Over the last decade, lead halide perovskites have emerged as a true 'superstar' among semiconducting materials. Due to their simple, cost-efficient synthesis and processing, their structural and thus, optical/electrical adjustability, lead halide perovskites have found application in many types of devices, such as photovoltaic cells [1–3], solid state lasers [4,5], light emitting diodes [6], photodetectors [7] and solar fuels production [8]. Additionally to thin films and single crystal lead halide perovskite, nanosized perovskites deserve a particular interest, since the facile perovskite lattice crystallization allows the preparation of various types of nanoparticles and nanostructures, including spherical nanoparticles [9], nanoplatelets [10], nanorods [11], or nanowires [12], among others. Perovskite nanostructures could display extraordinary photoluminescence quantum yield (PLQY) close to 100%, related to the charge confinement and lower defect concentration, as reported recently by S. Gonzalez-Carrero et al. [13] However, charge transport properties of perovskite nanostructures are usually behind those of 3D bulk perovskites [14]. One of the main issues, which hinders the utilization of perovskite nanoparticles (PNP) for certain electrical application, is the non-efficient screening of the electron–hole Coulomb interaction, as compared

* Corresponding author.
** Corresponding author.
E-mail addresses: yolanda.salinas@jku.at (Y. Salinas), kovalenko.alx@gmail.com (A. Kovalenko).

https://doi.org/10.1016/j.mtchem.2020.100272

to bulk materials. In fact, nanoparticles surrounded by an organic medium present a smaller dielectric constant [15] that has an exciton binding energy in the range of 200–500 meV [16], which is an order of magnitude higher in comparison with the bulk perovskites [17]. Thus, the higher exciton binding energy significantly reduces the exciton dissociation probability, prior to radiative decay as compared to the bulk, which results in a superior PLQY and poor charge transfer.

The preparation of peptide nucleic acids (PNAs) as synthetic analogues of naturally occurring nucleic acids [18,19] has attracted significant amount of interest in the last couple of decades. In contrast to deoxyribonucleic acids (DNAs), with a negatively charged chiral sugar-phosphate backbone, PNAs have a neutral and achiral pseudopeptide backbone consisting of *N*-(2-aminoethyl) glycine units. Moreover, the presence of the peptide backbone in PNA opens a path to simple chemical modifications and conjugation of various chemical groups, resulted from its chemical versatility and architectural flexibility. Similar to DNA, PNA forms duplex spiral with itself and other nucleic acids by Watson–Crick base pairing [20]. The weak distance dependence of the charge hopping mechanism and its prevalence in duplex drives the further potential exploration of charge transfer through PNA units. So far, several groups have already reported the charge transfer in PNA-metal complexes [21], the possible numerous PNA modifications [22], the self-assembling of PNA layers [23] and the formation of PNA/DNA ensembles [24]. Therefore, the unique properties exhibited by PNA recently attracted a considerable attention, not only in biomolecular applications but also in materials sciences and nanotechnology [25].

In this work, we introduce a pioneering approach to stabilize PNP with thymine-based peptide nucleic acid prepared by ligand assisted precipitation technique [26], since PNA has much higher local dielectric constant than the organic materials [27] which could be beneficial in terms of charge transfer. The combination of both unique PNP and PNA materials properties could open a pathway towards new generation of applied functional materials which can be utilized as molecular machines, switches and logic gates, which may be designed using PNA stabilized PNP as components or as switching stimuli.

2. Materials and methods

Lead (II) bromide ($PbBr_2$ 99.999%), methylammonium bromide (MABr, 98%) and adenine (>99%) were purchased from Sigma Aldrich. Hexanoic acid (98%) was purchased from TCI. Solvents *N*,*N*-dimethylformamide (DMF), chloroform and toluene were of reagent grade (≥99.8%) and were purchased from VWR. All chemicals were used as received without any further purification steps. PNA monomer (PNA-M) and trimer (PNA-T) were synthetized according to the detailed procedure described in Supporting Information.

PNP were prepared via a ligand assisted precipitation technique [13,26]. Typically, the precursor solution was made by dissolving in DMF the blends of $PbBr_2$, MABr, PNA-M or PNA-T and hexanoic acid at molar ratios 1:1.1:0.8/0.4:9.5, respectively, related to precursor concentration of 0.027, 0.030, 0.022/0.011 and 0.26 mol/L, respectively. Then, the precursor solution (20 μL) was precipitated in a vial with 10 mL of an antisolvent (toluene or chloroform) placed in an ice bath (0–3 °C) while being stirred at 1000 rpm. After that, the resulted precipitate was isolated by centrifugation (5000 rpm for 10 min), and the supernatant was consequently discharged. Finally, the yielded solid materials **PNP-PNA-M** or **PNP-PNA-T** was redispersed in the corresponding solvent or dried by vacuum at 40 °C for further characterization.

For film preparation, the precursor solution (50 μL) was precipitated in toluene (25 mL) in an ice bath while being stirred at 1000 rpm. A glass substrate was placed into the centrifugation tube and the PNP were centrifugal casted onto the substrate. The supernatant was discharged and then the film was dried on a hot plate at 40 °C in ambient conditions.

For adenine-binding tests, colloidal solutions were prepared by precipitation of PNA-M precursor solution (50 μL) in toluene (50 mL) in an ice bath. Then, adenine in various concentrations (0, 20, 60 and > 100% to the amount of thymine-based PNA-M) was added to the dispersion in order to test adenine sensing abilities of the PNP. The mixture was subsequently stirred at room temperature for 5 h, in order to induce hydrogen bonding between adenine and thymine group from the PNA-M molecules.

High-resolution transmission electron microscopy (HRTEM) images and energy dispersive X-ray spectroscopy (EDS) elemental mapping were obtained with Titan (FEI) microscope using Holey carbon film 300 Mesh copper grids. ImageJ software was used to determine the average particles size distribution from ca. 200 measurements from TEM images. Fourier-transform infrared spectroscopy (FTIR) spectra were recorded on a PerkinElmer Spectrum 100. Powder X-ray diffraction (XRD) measurements were performed on a Empyrean (PANalytical) diffractometer using Cu Kα (1.540598 Å) radiation at a voltage of 40 kV and 30 mA. To obtain solid material for powder XRD characterization, colloidal solutions were prepared by precipitation of precursor solution (1 mL) in toluene (50 mL) under cold conditions (0–3 °C), followed by centrifugation (5000 rpm for 10 min). Supernatant was discharged and the solid material was dried in a vacuum oven (40 °C) overnight. Ultraviolet–Visible (UV–Vis) and fluorescence spectroscopy were used to characterize the optical properties of the PNP. UV–Vis spectroscopy was carried out with a Lambda 1050 UV/Vis/NIR spectrometer (PerkinElmer). Photoluminescent (PL) spectra were taken on a fluorimeter from Photon Technology International. UV–Vis and PL spectra of colloidal PNP suspensions were measured in a 1 × 1 cm quartz cuvette. For the optical characterization the films were exposed to the 405 nm excitation wavelength at 50° angle. PLQY of PNP colloidal solutions and thin films were measured using integrating sphere Hamamatsu Photonics A9924-06, with Shamrock SR-303i monochromator and Andor iDus SiCCD detector. To characterize the surface morphology of the film, atomic force microscopy (AFM) (Bruker Innova) was used. For the temperature dependent optical measurements PNP thin films were placed in QuantumDesign DynaCool PPMS, COHERENT OBIS 405 excitation laser beam was supplied with a fiber optics with Shamrock SR-303i monochromator and Andor iStar DH320T-18U-73 charge couple device camera.

3. Results and discussion

In order to test the influence of the capping agent concentration on the PNP formation, different molar eq. of synthetized PNA-M to $PbBr_2$ were used in the preparation of the precursor solution (0.4, 0.8, 1.0 and 1.6 eq.). The PNP prepared with different amounts of capping agents were characterized by UV–Vis and PL spectroscopy (see Fig. SI-3). In all cases the colloidal solutions exhibited green light emission after UV irradiation, showing a yellowish color under visible light. For further experiments the PNA-M concentration selected was 0.8 eq. For the PNP precipitation optimization, three different molar ratios of hexanoic acid: $PbBr_2$ were chosen (0, 2.4 and 9.5), and the molar equivalents of the precursors selected were 1, 1.1 and 0.8 for $PbBr_2$, MABr and PNA-M, respectively. It was observed that when hexanoic acid was not present as capping agent, the prepared colloidal solution tended to aggregate immediately after the precipitation. Similarly, when 2.4 M ratio to $PbBr_2$ were added, the degradation of colloidal solution was faster. Therefore, the carboxylic acid molar ratio was maintained at 9.5, in

agreement with previously reported results by Perez-Prieto et al. [13] Furthermore, the influence of washing **PNP-PNA-M** after the preparation was tested. For that, the colloidal solution was centrifuged (5000 rpm for 10 min), the supernatant was discharged and the solid material was redispersed in the corresponding solvent (toluene or chloroform). Then, the crude and the washed colloidal solutions were tested by UV–Vis and PL spectroscopy observing that the washing did not cause any significant changes in the optical properties of the samples, as seen in Fig. SI-4.

The stabilization of PNP was also achieved by using a synthetized PNA-T (see experimental details in SI). In the accordance with the results obtained from **PNP-PNA-M**, nanoparticles **PNP-PNA-T** were prepared from precursor solutions with molar equivalents of 1, 1.1 and 9.5, for $PbBr_2$, MABr, and HeA respectively, whereas the molar equivalents of PNA-T varied from 0.4, 0.8 to 1.2. Interestingly, in this case, the molar equivalent of 1.2 eq. of PNA-T in precursor solution did not lead to the formation of PNP. Nevertheless, when molar equivalents 0.4 and 0.8 were used, yellow colloidal solutions with green emission were obtained (see in Fig. SI-5). Therefore, in this case 0.4 molar equivalents of PNA-T were selected for the formation of **PNP-PNA-T** nanoparticles, as shown in Fig. 1c-d, both for toluene (T) and chloroform (C) colloidal solutions.

UV–Vis and fluorescence spectroscopy were applied to characterize optically both **PNP-PNA-M** and **PNP-PNA-T** colloidal solutions, and their corresponding PLQY was determined. Initially, precursor solutions were precipitated in solvents toluene or chloroform to evaluate a possible solvent effect. **PNP-PNA-M** colloidal dispersion exhibited green-blue fluorescence with an emission maximum of 505 nm for both samples prepared in chloroform and toluene (see Fig. 1c). The PLQY values of the above mentioned colloidal solutions were 3 ± 2% and 6 ± 2% for the PNP dispersed in toluene and chloroform, respectively. PNP stabilized by PNA-trimer (**PNP-PNA-T**) exhibited red-shifted emission, at 528 and 518 nm for toluene and chloroform colloidal solution, respectively (see Fig. 1d), which corresponded to PLQY values between 0.5 and 1%. Obtained PLQY values were significantly lower in comparison to some already reported colloidal PNP suspensions [13]. Nevertheless, the formation of the particles at nanoscale size was proved by HRTEM (as it can be seen in Fig. 1e-f) and a similar average size of the nanoparticles formed was obtained for both nanomaterials **PNP-PNA-M** and **PNP-PNA-T** (9.4 ± 2.0 nm and 9.5 ± 2.3 nm, respectively). The nanoparticles size distribution and further nanoparticles HRTEM images are shown in Fig. SI-6. Worth noting that the distribution of the PNP size was affected by the TEM sample preparation, as far as during the drying process aggregations could occur, and the possible organic shell formed may be affected by local elevated temperatures during the measurements under the electron beam irradiation. The fast Fourier transform (FFT) pattern of TEM images confirmed the crystalline structure. Additionally, energy dispersive X-Ray spectroscopy (EDS) was used to semi-quantitatively confirm the composition of the nanoparticles. A significant presence of elements Br, Pb, C, O, and N were detected in the PNPs, as seen in the TEM–EDS–elemental mapping images (see Fig. 1g and Fig. SI-8). Approximately all the elements were homogeneously distributed among the sample, proving that no random aggregates were formed, except for a lead-rich area detected at the one of the NPs edges (more apparent in the merged image of Fig. 1g), what could indicate a possible Pb(0) surface passivation of PNPs [28]. Copper was not considered in the analysis since these elements are present in the TEM sample holder and traces of Si

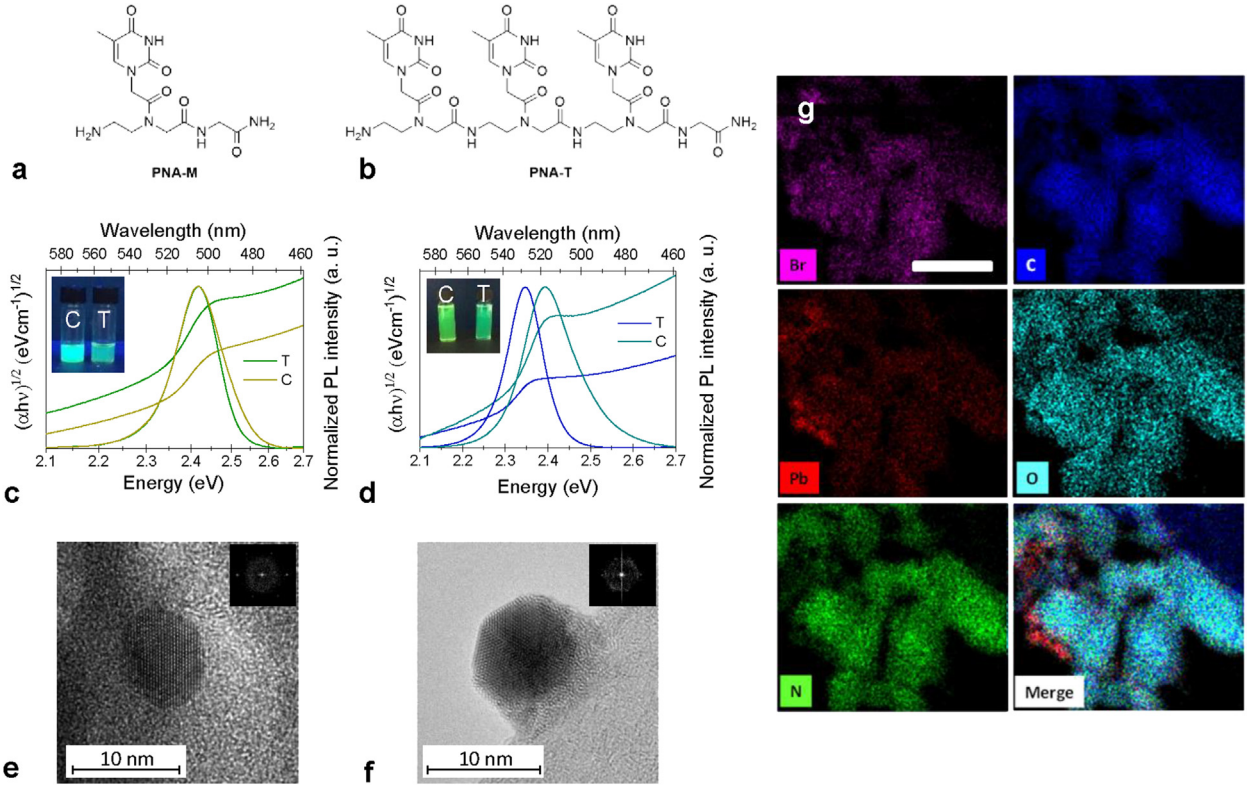

Fig. 1. a) Structure of PNA-monomer (PNA-M) and b) of PNA-trimer (PNA-T); c) UV-VIS and PL spectra of colloidal solutions of **PNP-PNA-M** (0.8 mol eq. of PNA-M), inset photo of colloidal solutions under UV irradiation in chloroform (C) and toluene (T); d) UV-VIS and PL spectra of colloidal solutions of **PNP-PNA-T** (0.4 mol eq. of PNA-T), inset photo of colloidal solutions under UV irradiation; e) TEM image of **PNP-PNA-M**, scale bar 10 nm, inset: FFT image; f) TEM image of **PNP-PNA-T**, scale bar 10 nm, inset: FFT image; and g) TEM–EDS–elemental mapping images of **PNP-PNA-T**, scale bar = 100 nm.

were neglected from likely handling contamination during TEM sample preparation.

The perovskite structure was verified by powder XRD spectroscopy (spectra shown in Fig. SI-7). Peaks corresponding to the reflections (001), (011), (111), (002), (021), (211), (220) and (300) were observed at positions 14.88°, 21.11°, 25.93°, 30.03°, 33.68, 37.00°, 43.00° and 45.74° respectively. In general, the XRD patterns were in a good agreement with previously reported results [29,30] and confirmed the cubic unit cell structure of the PNP. The broadening of the peaks observed for the nanomaterial **PNP-PNA-M** was attributed to the decreasing crystallite size.

Additionally, in order to further investigate the stabilization of nanoparticles through the PNA-based ligands interaction in the precursor solvent, Fourier-transform infrared (FTIR) spectroscopy was selected alongside with density functional theory (DFT) calculations. For that, the nanoparticles stabilization can be executed by the PNA monomer coordination to the PNP surface through two ways: by the primary amine or by the primary amide group, as it can be observed from the molecular structure of the PNA-M (Fig. 2). Assuming that the precursor reagents form coordination complexes already in the solution [31], they were modeled here using Gaussian 09 software package relative systems: Model #1 and Model #2 (see Fig. 2). As the criteria of the geometrical preferences, free Gibbs energy was considered. For the geometry optimization the 6 311+G* with split-valence polarized triple-ζ basis set polarization and diffuse functions on heavy atoms for C, N, H and O atoms, and Los Alamos National Laboratory 2 Double-ζ (LANL2DZ) was used for Pb and Br atoms. The SCRF procedure was applied to take into account effect of the solvent (DMF). Force constants and the resulting vibrational frequencies were computed in order to simulate IR spectra of the complexes. Comparing above mentioned model #1 and model #2, it could be observed that when PNA-M is coordinated to the $PbBr_3^-$ group by the primary amide (model #2) intermolecular H-bond is formed between the carbonyl group of the thymine and NH_3^+ group from the amide. Moreover, model #1 was more energetically favorable by 0.72 eV than model #2. Due to high computational costs the simulation was performed solely for PNA-M molecules, considering structural similarities to PNA-T.

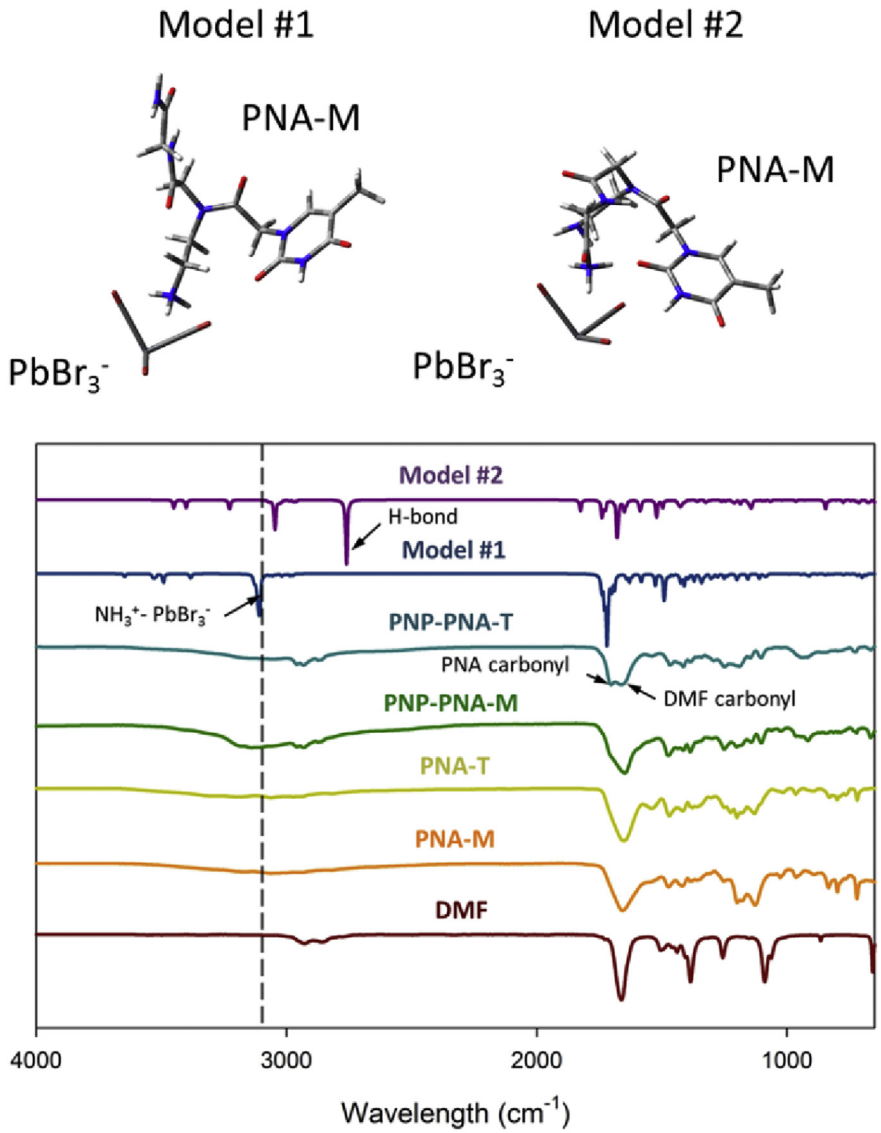

Fig. 2. FTIR spectra of PNP and their ligands and model #1 and #2 simulations that are attributed to the presence of ligands on the surface of PNP.

For unveiling the formation mechanism of the PNP in presence of PNA-M and PNA-T as ligands (**PNP-PNA-M** and **PNP-PNA-T** nanomaterials), the FTIR spectra of the precursor solutions and the nanomaterials were measured (Fig. 2) [32]. Characteristic signals from PNA-M and PNA-T were detected and main groups appeared at similar wavelengths, as expected from their chemical structure. In PNA-M a band at 3140 cm^{-1} was assigned to the N–H from amide I, whereas 1537 and 1520 cm^{-1} peaks belonged to stretching C–N and broadening N–H from the amide II in both precursors. This peak was slightly bigger for PNA-T since its structure contained three N–H groups (secondary amide). Carbonyl vibrations (C=O) from this secondary amide appeared at 1661 and 1651 cm^{-1} for PNA-M and PNA-T respectively, whereas C–N stretching (amide III) were visible at 1251 cm^{-1} in both PNA-based precursors. Two broad bands located between 3350 and 3150 cm^{-1} could be assigned to the N–H stretching of the primary amide. Interestingly, two broad peaks between 1670 and 1705 cm^{-1} were detected in both PNA-based PNP, which were assigned to the carbonyl group from PNA precursor and to solvent traces. The three main characteristic peaks from MABr were assigned at 2700-3300 cm^{-1} (broad signal, Br–H) and 1000 (narrow) and 912 cm^{-1} (medium) signals due to the C–H rocking bonds [33,34]. Those signals were slightly detected in both prepared PNPs, nevertheless, those bands could also be attributed to the primary ammonium salt of the PNA. Since PNA related absorption peaks were successfully observed in each corresponding prepared PNP, simulated and measured FTIR spectra were compared and it was observed that in case of the simulated spectrum of model #2, intramolecular H-bond results in strong characteristic peak at ~2800 cm^{-1}, which is absent in the measured spectra of PNP. Moreover, overall deformation of the PNA-M molecule results in shift of the main peaks (NH_3^+ coordinated to $PbBr_3^-$ present as a wide peak at ~3200 cm^{-1} and carbonyl group of thymine moiety). Therefore, it can be assumed that model #1 corresponds to the complex formed in the solution, thus PNA is most likely bonded to the PNP surface by the coordinate bond by the primary amine, concluding that the thymine group is directed outwards and its functionality is preserved.

Thin films were prepared from PNP dispersion by centrifugal casting method. Generally, as opposed to the spin casting of the same materials, films prepared by centrifugal casting method are densely packed and uniform (Fig. 3b and c). The films were characterized by UV–Vis and PL spectroscopy. The emission maximum for **PNP-PNA-M** and for **PNP-PNA-T** was 519 and 531 nm, respectively. In general, emission peak of the films was red-shifted when compared to the colloidal solutions, assumingly due to the partial aggregation. The results were summarized in Table 1. Furthermore, as expected, the PLQY of the **PNP-PNA-M** and of **PNP-PNA-T** films were around 0.5 and 0.4%, respectively, what is a lower value than determined for the colloidal solutions. That could be explained by assuming that bulky non crystalline capping agents may result in the presence of intrinsic defects in the perovskite lattice, which can act as charge traps and quench luminescence. Similarly, in our previous works we already observed that during the photoexcitation the charge carrier could be transferred to the surface ligand due to the presence of strong electron acceptors [35]. Furthermore, AFM was used to probe the surface modification of the glass support with **PNP-PNA-M** (see topographic image in Fig. SI-9). The root-mean-square (RMS) roughness (Rq) value was 97 nm which could be an indication of the inhomogeneous overcoat.

Remarkably, the films stored in the ambient conditions (room temperature and humidity of 40–50%) after 32 days possessed a slight red shift in the emission maximum from initial 517 nm–523 nm, see in Fig. 3d which most likely caused by the PNP aggregation, however taking into account perovskite sensitivity to

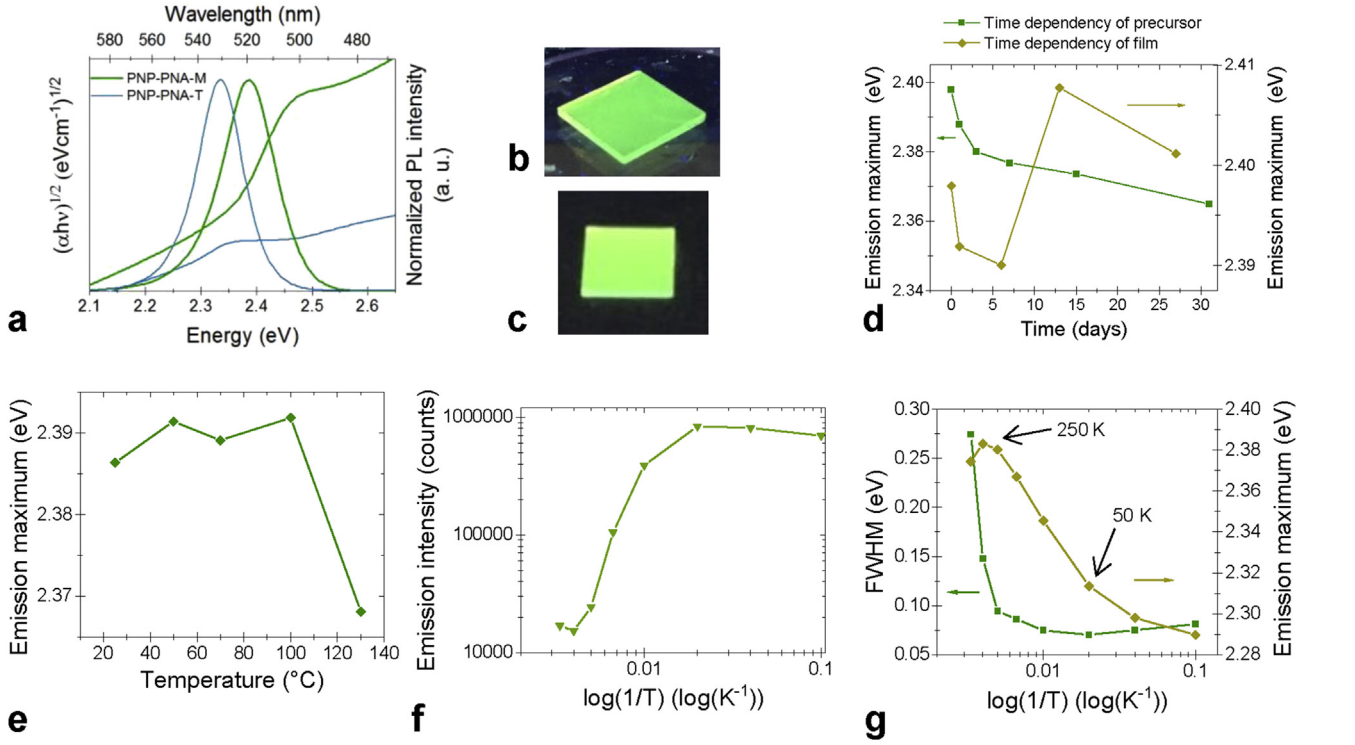

Fig. 3. a) UV-VIS and PL spectra of **PNP-PNA-M** and **PNP-PNA-T** thin films, b) a photo of **PNP-PNA-M** thin film under UV irradiation (366 nm), c) a photo of **PNP-PNA-T** thin film under UV irradiation (366 nm), d) a stability study of **PNP-PNA-M** thin films, an influence of the film's age on PL emission and an influence of the precursor solution's age on PL emission, e) an influence of temperature on **PNP-PNA-M** thin films PL emission, f) an influence of low temperature on **PNP-PNA-M** thin films PL emission, g) an influence of low temperature on **PNP-PNA-M** thin films PL maximum and full width at half maximum (FWHM) with an inset of temperature of the lattice transformation from orthorhombic (around 250 K) to tetragonal (around 50 K) and then to cubic.

Table 1
Summary of optical data obtained from spectroscopic characterization of nanoparticles **PNP-PNA-M** and **PNP-PNA-T** by different sample preparations.

	Nanoparticles sample	Emission maximum (nm/eV)	Bandgap (eV)	FWHM (eV)	PLQY (%)
PNP-PNA-M	Chloroform solution	505/2.42	2.35	0.132	5 ± 1
	Toluene solution	505/2.42	2.33	0.118	2 ± 1
	Thin film	519/2.39	2.37	0.113	0.5 ± 0.2
PNP-PNA-T	Chloroform solution	518/2.39	2.31	0.142	1.0 ± 0.5
	Toluene solution	528/2.35	2.28	0.097	0.5 ± 0.2
	Thin film	531/2.33	2.28	0.097	0.4 ± 0.2

moisture [36] overall temporal stability can be considered to be quite satisfactory. Annealing temperature stability test of the samples prepared by centrifugal casting was depicted in Fig. 3e. It is worth to be noted that no significant changes in the luminescence intensity were observed at the annealing temperature below 100 °C. However, for the samples annealed at 130 °C and above, a red shift in the emission maximum was detected. Hence, it can be assumed that PNP start to aggregate at high temperatures due to the dynamical surface instability. Therefore, the precursor solution stability was tested and colloidal dispersions were prepared at different time frames from: fresh; 2 days; 1 week; 2 weeks and 4 weeks old precursor solutions. Precursor solutions were stirred at ambient conditions before the precipitation. As it is shown in Fig. 3d, emission maximum was slightly blue shifted with the increasing age of the precursor solution. Presumably, additional moisture from the atmosphere could have affected the perovskite crystallization process since the precursor solutions were stored under ambient conditions [37,38].

We assumed that low PLQY values, when compared to previously reported works [13], was caused by preferred non-radiative relaxation processes in PNP. Thus, PL spectra of **PNP-PNA-M** thin films were measured at various temperatures, varying from 300 K to 10 K. As expected, with decreasing temperature the PL intensity (see Fig. 3f and Fig. SI-10) increased by three orders of magnitude which could confirm reducing the non-radiative relaxation processes by lowering the temperature and thus, increasing of PLQY [39]. Moreover, with decreasing temperature, it was observed an emission maxima shifting from 536 nm (2.37 eV) at 300 K to 555 nm (2.29 eV) at 10 K and simultaneously, the FWHM was decreasing (see Fig. 3g). This observation is in agreement with previously reported results [40]. The emission maximum shift was probably caused by the lattice transition from cubic to tetragonal (around 50 K) and then to orthorhombic (around 250 K), as it can be observed in Fig. 3g.

Charge transfer between nucleic acids is a well-known phenomenon in both PNA and DNA [41,42] as a result of hopping of the

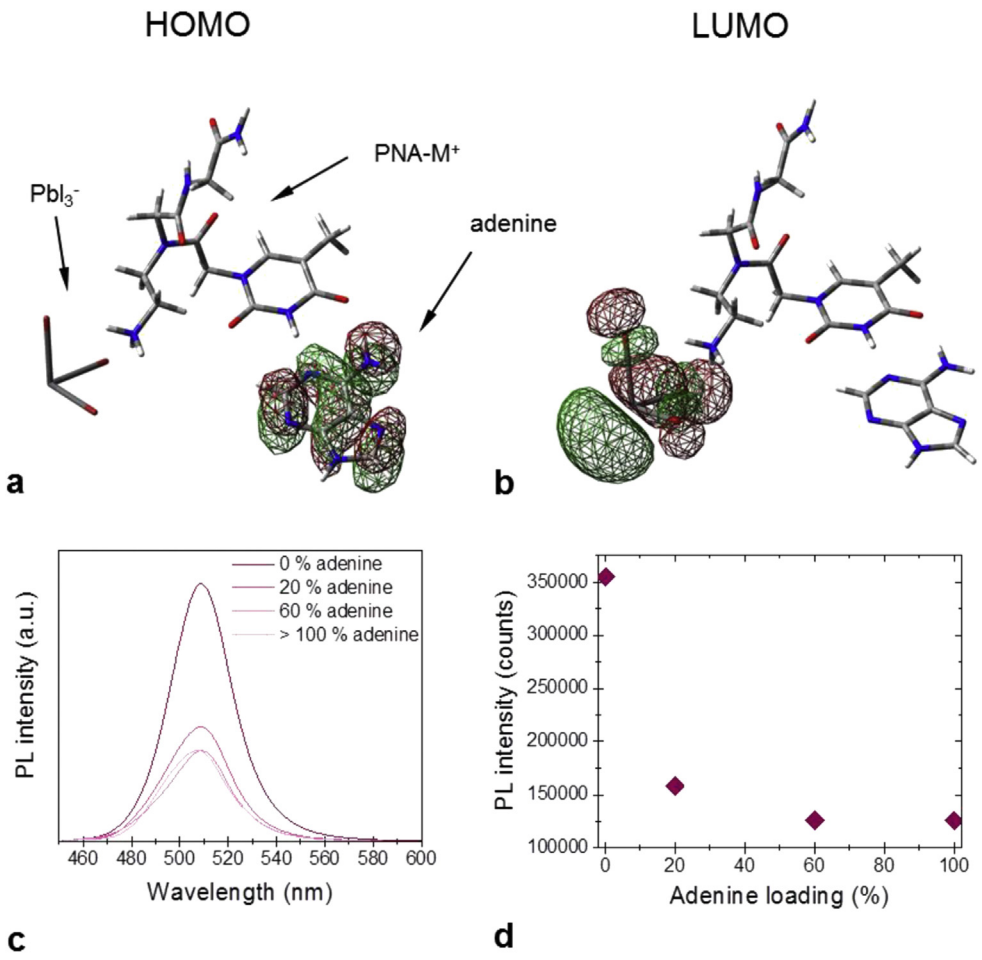

Fig. 4. Model of binding adenine to PNA^{+}-PbI_3 electron density at HOMO (a) and LUMO (b) energy orbitals; (c) PL spectra and (d) PL intensity vs. adenine loading (c).

Table 2
Optical characterization of **PNP-PNA-M** with different adenine loadings.

Adenine conc. (mol/L)	Adenine loading (%)	$\lambda_{em,\ max}$ (nm)	PL intensity (a. u.)
0	0	509	354 000
$4.4 \cdot 10^{-6}$	20	509	157 000
$1.3 \cdot 10^{-5}$	60	509	126 000
$3.7 \cdot 10^{-5}$	100	507	126 000

charge carriers between the nucleic acids on the peptide backbone. Therefore, in the present case to consider this phenomenon, adenine nucleic acid was added to the colloidal solution, as far as the thymine moiety is supposed to be dangling out of the nanoparticles surface and its functionality, i.e. its affinity to adenine molecules as complementary base, should be preserved. Complementary pairs are coupled to each other via hydrogen bonding and it can be expected that bonding of adenine units to PNP surface modified with thymine moieties would cause a PL quenching by the charge transfer, as reported for the luminescence quenching by photo induced charge transfer between metal complexes in peptide nucleic acids [43]. Thus, adenine was added into the toluene colloidal solution in various molar ratios (0%, 20%, 60% and 100%) with a respect to the amount of thymine-based PNA-M ligand. The colloidal solutions were stirred for ca. 5 h, at ambient conditions, to induce the hydrogen bonds formation. For each sample, the emission was measured and PL peak intensity was taken (see Fig. 4c and Table 2). For the measurement clarity, all the samples were measured at the same setting of the instrument. It was found out that the addition of adenine notably decreased the intensity of fluorescence emission of the nanoparticles **PNP-PNA-M**. Interestingly, emission maxima did not change when adenine was added into the colloidal solution. The limit of detection was found to be 1.76 ppm of adenine (60% addition, see Table 2, and Fig. 4d) which is comparable with other reported nucleic acid sensors [43]. The PNA selected in this work contained thymine, which complementary pairs may bound to each other via hydrogen bonding. Hence, it was also expected that bonding of adenine to PNP surface modified with thymine moieties would cause PL quenching due to the charge transfer [44].

To explain the possible mechanism of the luminescence quenching complex of the $PbBr_3^-$ PNA^+ with an adenine H-bonded to thymine group of PNA, a model of binding was used (Fig. 4a and b). Concerning the electron density distribution in the complex, it was observed that in the ground state the electron at the highest occupied molecular orbital (HOMO) was fully localized at the adenine molecule. However, the electron density at the lowest unoccupied molecular orbital (LUMO) was displaced to the $PbBr_3^-$ (Fig. 4a and b). Considering the dominant hole mobility in the methylammonium lead bromide perovskite [45], it could be assumed that the photogenerated charge carrier is transferred between the PNP surface ligands and H-bonded adenine, which resulted in a luminescence quenching.

Conclusions

In conclusion, peptide nucleic acid monomer- and trimer-stabilized perovskite nanoparticles (**PNP-PNA-M** and **PNP-PNA-T**) were successfully prepared. This type of nanoparticles can be centrifuged, washed and re-dispersed without any significant changes in their spectral properties. Their perovskite crystallinity was confirmed by XRD and **PNP-PNA-M** and **PNP-PNA-T** colloidal dispersions in chloroform and toluene exhibited green-blue fluorescence. Quantum chemical calculations showed that formation of the coordination bond between primary amine group and PNP surface is the preferred orientation, thus PNA containing thymine groups on PNP surface are exposed outwards. One of the interesting features of these nanoparticles is the luminescence quenching by the addition of adenine via charge transfer, with a limit of detection close to 2 ppm was obtained. Additionally, thin films were prepared by centrifugal casting and its potential optical features confirmed the possible preparation of PNA-based films for future applications. The high chemical versatility of PNA ligands could allow expanding the described approach for the sensing of whole spectrum of nucleic acids including DNA sequences. In general, ligand-assisted precipitation is an extremely facile method to prepare perovskite nanoparticles due to moderate operational temperature, conventional chemicals and large versatility of capping agents that can be used [46]. We believe that this approach can open a path towards numerous possibilities of combining the unique properties of PNA as molecular building blocks in nanotechnology and perovskites as promising nanomaterials for applications in electronics.

Declaration of competing interest

The authors declare that they have no known competing financial interests or personal relationships that could have appeared to influence the work reported in this paper.

Acknowledgements

The authors want to thank Prof. Markus Himmelsbach (Johannes Kepler University, Institute for Analytical Chemistry) for his help regarding the mass spectrometry measurements. We acknowledge the support by the Operational Program Research, Development and Education – European Regional Development Fund (Project No. CZ.02.1.01/0.0/0.0/16_019/0000754) of the Ministry of Education, Youth and Sports of the Czech Republic, and the project No. 19-23718S by the Czech Science Foundation. We gratefully acknowledge the financial support of Austrian Science Funds FWF within the Wittgenstein Prize (Z222 N19) for Prof. N. S. Sariciftci.

Author contribution statements

A.J.P. and Y.S conceived of the presented idea. A.J.P carried out all the PNP preparations and performed all the optical characterization and help writing the manuscript. S.G synthetized and characterized the PNA-based ligands. A.K. developed the theory, wrote the manuscript and performed the computations. M.C.S arranged and optimized the PL measurement set up. M.C.S and C.Y. verified the analytical methods. K.C. and R.Z. captured HRTEM images of the PNPs. Y.S. assisted further TEM measurements and contributed to characterizations such as FT-IR, sensing, size distribution analysis. N.S.S., J.K., M.W., and O.B. supervised the findings of this work. All authors provided critical feedback and helped shape the research, analysis and manuscript.

Appendix A. Supplementary data

Supplementary data to this article can be found online at https://doi.org/10.1016/j.mtchem.2020.100272.

References

[1] Z. Shi, A.H. Jayatissa, Perovskite-based solar cells: a review of recent progress, materials and processing methods, Materials 11 (2018) 729, https://doi.org/10.3390/ma11050729.
[2] B. Dou, J.B. Whitaker, K. Bruening, D.T. Moore, L.M. Wheeler, J. Ryter, N.J. Breslin, J.J. Berry, S.M. Garner, F.S. Barnes, S.E. Shaheen, C.J. Tassone, K. Zhu, M.F.A.M. van Hest, Roll-to-Roll printing of perovskite solar cells, ACS Energy Lett. 3 (2018) 2558–2565, https://doi.org/10.1021/acsenergylett.8b01556.
[3] S. Tombe, G. Adam, H. Heilbrunner, C. Yumusak, D.H. Apaydin, B. Hailegnaw, C. Ulbricht, C.J. Arendse, H. Langhals, E. Iwuohaa, N.S. Sariciftci, M.C. Scharber, The influence of perovskite precursor composition on the morphology and

photovoltaic performance of mixed halide $MAPbI_3$-xClx solar cells, Sol. Energy 163 (2018) 215–223, https://doi.org/10.1016/j.solener.2018.01.083.
[4] Q. Liao, X. Jin, H. Fu, Tunable halide perovskites for miniaturized solid-state laser applications, Adv. Opt. Mater. (2019), https://doi.org/10.1002/adom.201900099.
[5] A. Zhizhchenko, S. Syubaev, A. Berestennikov, A.V. Yulin, A. Porfirev, A. Pushkarev, I. Shishkin, K. Golokhvast, A.A. Bogdanov, A.A. Zakhidov, A.A. Kuchmizhak, Y.S. Kivshar, S.V. Makarov, Single-mode lasing from imprinted halide-perovskite microdisks, ASC Nano (2019), https://doi.org/10.1021/acsnano.8b08948.
[6] K. Lin, J. Xing, L.N. Quan, F.P.G. de Arquer, X. Gong, J. Lu, L. Xie, W. Zhao, D. Zhang, C. Yan, W. Li, X. Liu, Y. Lu, J. Kirman, E.H. Sargent, Q. Xiong, Z. Wei, Perovskite light-emitting diodes with external quantum efficiency exceeding 20 per cent, Nature 562 (2018) 245—248, https://doi.org/10.1038/s41586-018-0575-3.
[7] L. Dou, Y. Yang, J. You, Z. Hong, W.-H. Chang, G. Li, Y. Yang, Solution-processed hybrid perovskite photodetectors with high detectivity, Nat. Commun. 5 (2014) 5404, https://doi.org/10.1038/ncomms6404.
[8] Y.-S. Chen, J.S. Manser, P.V. Kamat, All solution-processed lead halide perovskite-BiVO4 tandem assembly for photolytic solar fuels production, J. Am. Chem. Soc. 137 (2015) 974–981, https://doi.org/10.1021/ja511739y.
[9] L.C. Schmidt, A. Pertegas, S. Gonzalez-Carrero, O. Malinkiewicz, S. Agouram, G. Minguez Espallargas, H.J. Bolink, R.E. Galian, J. Perez-Prieto, Nontemplate synthesis of CH3NH3PbBr3 perovskite nanoparticles, J. Am. Chem. Soc. 136 (2014) 850–853, https://doi.org/10.1021/ja4109209.
[10] M.C. Weidman, A.J. Goodman, W.A. Tisdale, Colloidal halide perovskite nanoplatelets: an exciting new class of semiconductor nanomaterials, Chem. Mater. 29 (2017) 5019–5030, https://doi.org/10.1021/acs.chemmater.7b01384.
[11] S. Aharon, L. Etgar, Two dimensional organometal halide perovskite nanorods with tunable optical properties, Nano Lett. 16 (2016) 3230–3235, https://doi.org/10.1021/acs.nanolett.6b00665.
[12] J. Feng, C. Gong, H. Gao, W. Wen, Y. Gong, X. Jiang, B. Zhang, Y. Wu, Y. Wu, H. Fu, L. Jiang, X. Zhang, Single-crystalline layered metal-halide perovskite nanowires for ultrasensitive photodetectors, Nat. Electron. 1 (2018) 404–410, https://doi.org/10.1038/s41928-018-0101-5.
[13] S. Gonzalez-Carrero, M. Martinez-Sarti, M. Sessolo, R.E. Galian, J. Perez-Prieto, Highly photoluminescent, dense solid films from organic-capped $CH_3NH_3PbBr_3$ perovskite colloids, J. Mater. Chem. C. 6 (2018) 6771–6777, https://doi.org/10.1039/C8TC01344F.
[14] Yuanyuan Dong, Yizhou Zhao, Siyu Zhang, Yi Dai, Lang Liu, Yujing Li, Qi Chen, J. Mater. Chem. 6 (2018) 21729–21746, https://doi.org/10.1039/C8TA06376A.
[15] Solmaz Torabi, Fatemeh Jahani, Ineke Van Severen, Catherine Kanimozhi, Satish Patil, W. Remco, A. Havenith, Ryan C. Chiechi, Laurence Lutsen, J. Dirk, M. Vanderzande, Thomas J. Cleij, Jan C. Hummelen, L. Jan Anton Koster, Adv. Funct. Mater. 25 (2015) 150–157, https://doi.org/10.1002/adfm.201402244.
[16] Ho-Wa Li, Zhiqiang Guan, Yuanhang Cheng, Taili Lui, Qingdan Yang, Chun-Sing Lee, Song Chen, Sai-Wing Tsang, Adv. Electron. Mater. 2 (2016), 1600200, https://doi.org/10.1002/aelm.201600200.
[17] Atsuhiko Miyata, Anatolie Mitioglu, Paulina Plochocka, Portugall Oliver, Jacob Tse-Wei Wang, Samuel D. Stranks, Henry J. Snaith, Robin J. Nicholas, Nat. Phys. 11 (2015) 582–587, https://doi.org/10.1038/NPHYS3357.
[18] P.E. Nielsen, M. Egholm, R.H. Berg, O. Buchardt, Sequence-selective recognition of DNA by strand displacement with a thymine-substituted polyamide, Science 254 (1991) 1497–1500, https://doi.org/10.1126/science.1962210.
[19] M. Egholm, O. Buchardt, P.E. Nielsen, R.H. Berg, Peptide nucleic acids (PNA). Oligonucleotide analogues with an achiral peptide backbone, J. Am. Chem. Soc. 114 (1992) 1895–1897, https://doi.org/10.1021/ja00031a062.
[20] M. Egholm, O. Buchardt, L. Christensen, C. Behrens, S.M. Freier, D.A. Driver, R.H. Berg, S.K. Kim, B. Norden, P.E. Nielsen, PNA hybridizes to complementary oligonucleotides obeying the Watson-Crick hydrogen-bonding rules, Nature 365 (1993) 566–568, https://doi.org/10.1038/365566a0.
[21] E. Wierzbinski, A. de Leon, K.L. Davis, S. Bezer, M.A. Wolak, M.J. Kofke, R. Schlaf, C. Achim, D.H. Waldeck, Charge transfer through modified peptide nucleic acids, Langmuir 28 (2012) 1971–1981, https://doi.org/10.1021/la204445u.
[22] E. Wierzbinski, A. de Leon, X. Yin, A. Balaeff, K.L. Davis, S. Reppireddy, R. Venkatramani, S. Keinan, D.H. Ly, M. Madrid, D.N. Beratan, C. Achim, D.H. Waldeck, Effect of backbone flexibility on charge transfer rates in peptide nucleic acid duplexes, J. Am. Chem. Soc. 134 (2012) 9335–9342, https://doi.org/10.1021/ja301677z.
[23] A. Paul, R.M. Watson, P. Lund, Y. Xing, K. Burke, Y. He, E. Borguet, C. Achim, D.H. Waldeck, Charge transfer through single-stranded peptide nucleic acid composed of thymine nucleotides, J. Phys. Chem. C 112 (2008) 7233–7240, https://doi.org/10.1021/jp711764q.
[24] E. Hatcher, A. Balaeff, S. Keinan, R. Venkatramani, D.N. Beratan, PNA versus DNA: effects of structural fluctuations on electronic structure and hole-transport mechanisms, J. Am. Chem. Soc. 130 (2008) 11752–11761, https://doi.org/10.1021/ja802541e.
[25] N.C. Seeman, Nucleic acid junctions and lattices, J. Theor. Biol. 99 (1982) 237–247, https://doi.org/10.1016/0022-5193(82)90002-9.
[26] F. Zhang, H. Zhong, C. Chen, X. Wu, X. Hu, H. Huang, J. Han, B. Zou, Y. Dong, Brightly luminescent and color-tunable colloidal CH3NH3PbX3 (X = Br, I, Cl) quantum dots: potential alternatives for display technology, ACS Nano 9 (2015) 4533–4542, https://doi.org/10.1021/acsnano.5b01154.
[27] V.N. Kadam, K. Saikrishnan, K.N. Ganesh, 5-Amidodansyl-U (U^D) peptide nucleic acid (PNA) as a fluorescent sensor of the local dielectric constant (ε) in PNA duplexes: major grooves in PNA duplexes are more hydrophobic than major grooves in DNA–DNA duplexes, J. Phys. Chem. C 122 (2018) 14004–14013, https://doi.org/10.1021/acs.jpcc.8b01098.
[28] A. Jancik Prochazkova, Y. Salinas, C. Yumusak, M.C. Scharber, O. Brüggemann, M. Weiter, N.S. Sariciftci, J. Krajcovic, A. Kovalenko, Controlling quantum confinement in luminescent perovskite nanoparticles for optoelectronic devices by the addition of water, ACS Appl. Nano Mater. 3 (2020) 1242–1249, https://doi.org/10.1021/acsanm.9b01857.
[29] A. Kovalenko, J. Pospisil, O. Zmeskal, J. Krajcovic, M. Weiter, Ionic origin of a negative capacitance in lead halide perovskites, Phys. Status Solidi RRL 11 (2017), 1600418, https://doi.org/10.1002/pssr.201600418.
[30] K.-H. Wang, L.-C. Li, M. Shellaiah, K. Wen Sun, Structural and photophysical properties of methylammonium lead tribromide ($MAPbBr_3$) single crystals, Sci. Rep. 7 (2017) 1–14, https://doi.org/10.1038/s41598-017-13571-1.
[31] J.-W. Lee, Z. Dai, C. Lee, H.M. Lee, T.-H. Han, N. De Marco, O. Lin, C.S. Choi, B. Dunn, J. Koh, D. Di Carlo, J.H. Ko, H.D. Maynard, Y. Yang, Tuning molecular interactions for highly reproducible and efficient formamidinium perovskite solar cells via adduct approach, J. Am. Chem. Soc. 140 (2018) 6317–6324, https://doi.org/10.1021/jacs.8b01037.
[32] Y. Hassan, O.J. Ashton, J.H. Park, G. Li, N. Sakai, B. Wenger, A.-A. Haghighirad, N.K. Noel, M.H. Song, B.R. Lee, R.H. Friend, H.J. Snaith, Facile synthesis of stable and highly luminescent methylammonium lead halide nanocrystals for efficient light emitting devices, J. Am. Chem. Soc. 141 (3) (2019) 1269–1279, https://doi.org/10.1021/jacs.8b09706.
[33] H. Sun, Z. Yang, M. Wie, W. Sun, X. Li, S. Ye, Y. Zhao, H. Tan, E.L. Kynaston, T.B. Schon, et al., Chemically addressable perovskite nanocrystals for light-emitting applications, Adv. Mater. 29 (2017), 1701153, https://doi.org/10.1002/adma.201701153.
[34] A. Ebrahiminezhad, Y. Ghasemi, S. Rasoul-Amini, J. Barar, S. Davaran, Impact of amino-acid coating on the synthesis and characteristics of iron-oxide nanoparticles (IONs), Bull. Kor. Chem. Soc. 33 (2012) 3957–3962, https://doi.org/10.5012/bkcs.2012.33.12.3957.
[35] A. Jancik Prochazkova, Y. Salinas, C. Yumusak, O. Brüggemann, M. Weiter, N.S. Sariciftci, J. Krajcovic, A. Kovalenko, Cyclic peptide stabilized lead halide perovskite nanoparticles, Sci. Rep. 9 (2019), 12966-12966.
[36] C. Müller, T. Glaser, M. Plogmeyer, M. Sendner, S. Döring, A.A. Bakulin, C. Brzuska, R. Scheer, M.S. Pshenichnnikov, W. Kowalsky, A. Pucci, R. Lovrinčič, Water infiltration in methylammonium lead iodide perovskite: fast and inconspicuous, Chem. Mater. 27 (2015) 7835–7841, https://doi.org/10.1021/acs.chemmater.5b03883.
[37] X. Zhou, Y. Zhang, W. Kong, M. Hu, L. Zhang, C. Liu, X. Li, C. Pan, G. Yu, C. Cheng, B. Xu, Crystallization manipulation and morphology evolution for highly efficient perovskite solar cell fabrication via hydration water induced intermediate phase formation under heat assisted spin-coating, J. Mater. Chem. A. 6 (2018) 3012–3021, https://doi.org/10.1039/C7TA08947C.
[38] X. Gong, M. Li, X.-B. Shi, H. Ma, Z.-K. Wang, L.-S. Liao, Controllable perovskite crystallization by water additive for high-performance solar cells, Adv. Funct. Mater. 25 (2015) 6671–6678, https://doi.org/10.1002/adfm.201503559.
[39] H.C. Woo, J.W. Choi, J. Shin, S.-H. Chin, M.H. Ann, C.-L. Lee, Temperature-dependent photoluminescence of $CH_3NH_3PbBr_3$ perovskite quantum dots and bulk counterparts, J. Phys. Chem. Lett. 9 (2018) 4066–4074, https://doi.org/10.1021/acs.jpclett.8b01593.
[40] Y. Liu, H. Lu, J. Niu, H. Zhang, S. Lou, C. Gao, Y. Zhan, X. Zhang, Q. Jin, L. Zheng, Temperature-dependent photoluminescence spectra and decay dynamics of $MAPbBr_3$ and $MAPbI_3$ thin films, AIP Adv. 8 (2018), 095108, https://doi.org/10.1063/1.5042489.
[41] R. Venkatramani, S. Keinan, A. Balaeff, D.N. Beratan, Nucleic acid charge transfer: black, white and gray, Coord. Chem. Rev. 255 (2011) 635–648, https://doi.org/10.1016/j.ccr.2010.12.010.
[42] E. Wierzbinski, A. de Leon, K.L. Davis, S. Bezer, M.A. Wolak, M.J. Kofke, R. Schlaf, C. Achim, D.H. Waldeck, Langmuir 88 (2012) 1971–1981, https://doi.org/10.1021/la204445u.
[43] Juewen Liu, Zehui Cao, Yi Lu, Functional Nucleic Acid Sensors, Chem. Rev. 109 (5) (2009) 1948–1998.
[44] X. Yin, J. Kong, A. de Leon, Y. Li, Z. Ma, E. Wierzbinski, C. Achim, D.H. Waldeck, Luminescence quenching by photoinduced charge transfer between metal complexes in peptide nucleic acids, J. Phys. Chem. B 118 (2014) 9037–9045, https://doi.org/10.1021/jp5027042.
[45] L.M. Herz, Charge-carrier mobilities in metal halide perovskites: fundamental mechanisms and limits, ACS Energy Lett. 2 (2017) 1539–1548, https://doi.org/10.1021/acsenergylett.7b00276.
[46] A. Jancik Prochazkova, S. Demchyshyn, C. Yumusak, J. Másilko, O. Brüggemann, M. Weiter, M. Kaltenbrunner, N.S. Sariciftci, J. Krajcovic, Y. Salinas, A. Kovalenko, Proteinogenic amino acid assisted preparation of highly luminescent hybrid perovskite nanoparticles, ACS Appl. Nano Mat. 2 (2019) 4267–4274.